ANALYSIS OF WETTING AND CONTACT ANGLE HYSTERESIS ON CHEMICALLY PATTERNED SURFACES

XIANMIN XU† AND XIAOPING WANG‡

Abstract. The wetting and contact angle hysteresis on chemically patterned surfaces in two dimensions are analyzed from a stationary phase-field model for immiscible two phase fluid. We first study the sharp interface limit of the model by the method of matched asymptotic expansions. We then justify the results rigorously by the Γ-convergence theory for the related variational problem and study the properties of the limiting minimizers. The results also provide a clear geometric picture of the equilibrium configuration of the interface. This enables us to explicitly calculate the total surface energy for the two phase systems on chemically patterned surfaces with simple geometries, namely the two phase flow in a channel and the drop spreading. By considering the quasi-static motion of the interface described by the change of volume (or volume fraction), we can follow the change of energy landscape which also reveals the mechanism for the stick-slip motion of the interface and contact angle hysteresis on the chemically patterned surfaces. As the interface passes through patterned surfaces, we observe not only stick-slip of the interface and switching of the contact angles but also the hysteresis of contact point and contact angle. Furthermore, as the size of the pattern decreases to zero, the stick-slip becomes weaker but the hysteresis becomes stronger in the sense that one observes either the advancing contact angle or the receding contact angle (when the interface is moving in the opposite direction) without the switching in between.

Key words. contact angle hysteresis, phase-field model, Γ-convergence

AMS subject classifications. 41A60,49J45,76T10

1. Introduction.

The study of wetting phenomenon is of critical importance for many applications and has attracted much interest in physics and applied mathematics communities, stimulated by the development of surface engineering and the studies on the superhydrophobicity property in a variety of nature and artificial objects [1, 11, 9, 18]. The primary parameter that characterizes wetting is the static contact angle, which is defined as the measurable angle that a liquid makes with a solid. The contact angle of liquid with a flat, homogenous surface is given by Young's equation[29]

$$\cos\theta = \frac{\gamma_{SV} - \gamma_{SL}}{\gamma}, \tag{1.1}$$

where γ_{SV}, γ_{SL} and γ are the surface tension of the solid-vapor interface, the solid-liquid interface and the liquid-vapor interface respectively. If the liquid wets the surface (referred to as wetting liquid or hydrophilic surface), the value of the static contact angle is $0 \le \theta \le 90^o$, whereas if the liquid does not wet the surface (referred to as nonwetting liquid or hydrophobic surface), the value of the contact angle is $90^o \le \theta \le 180^o$. Surfaces with a contact angle between 150^o and 180^o are called superhydrophobic.

Experimentally, the contact angle of a drop on rough surface has been observed to take a range of values. The highest (lowest) stable contact angle is termed the advancing (receding) angle θ_a (θ_r). The observed contact angle is usually velocity dependent and the advancing (receding) contact angle is defined in the limit of contact line velocity $U \to 0$ with $U > 0$ ($U < 0$) [10]. The contact angle hysteresis (CAH) $\Delta\theta = \theta_a - \theta_r$ proves to be an important quantity that determines many properties

†Institute of Computational Mathematics and Scientific/Engineering Computing, Chinese Academy of Sciences, Beijing 100080, China. (xmxu@lsec.cc.ac.cn).

‡Department of Mathematics, the Hong Kong University of Science and Technology, Clear Water Bay, Kowloon, Hong Kong, China. (mawang@ust.hk)

of the surface. The origin of CAH is attributed to several factors such as surface roughness, chemical contaminants, among others. Theoretical models of CAH have focused on roughness and heterogeneity as providing energy barriers for the system to attain the global minimum[9, 22].

In this paper, we study the wetting and hysteresis on chemically patterned surface based on a phase field model (2.8) (2.9) and the related variational problem. Using the method of matched asymptotic expansion, we first study the sharp interface limit of the solution to the phase field model. We show that the limit describes an interface with constant curvature that intersects the patterned surface with a contact angle θ_s. At the border point between the strips, the value of the contact angle is not unique. The asymptotic results can be justified rigorously by the Γ-convergence theory for the related variational problem and the careful study of the sharp-interface energy minimization problem. The Γ-convergence theory for the chemically homogeneous surface have been developed in [15][17]. We generalize the results to the case with chemically inhomogeneous surface energy density and prove the convergence of the minimizers of the diffuse interface problems to that of the sharp-interface problem. We also study the geometric property of the minimizers of the sharp-interface model. The result, which is a generalization of the result in [7] with zero surface energy, justifies what we have obtained by the asymptotic expansions.

Based on the sharp interface model, we then give a detailed investigate of the stick-slip motion of the interface and the contact angle hysteresis for two cases with chemically patterned surfaces, namely the quasi-static motion of the two phase flow in a channel and the quasi-static spreading of a liquid drop. By considering motion of the interface as the volume of the drop (or volume fraction of the two fluids) is quasi-statically increased or decreased, one can explicitly compute the energy functions in both cases. As the interface passes through patterned surfaces, we observe not only the stick-slip of the interface and the switching of the contact angles but also the hysteresis of contact point and contact angle. Furthermore, as the size of the pattern decreases to zero, the stick-slip becomes weaker but the hysteresis becomes stronger in the sense that one observes either the advancing contact angle or the receding contact angle (when the interface moving in the opposite direction) without the switching in between.

We remark that the dynamic hysteresis with finite interface speed (instead of quasi-static) was studied numerically in a recent work in [24]. We simulated the moving contact line in a two-dimensional chemically patterned channel using a diffuse-interface model with the generalized Navier boundary condition developed in [21]. The motion of the fluid-fluid interface in confined immiscible two-phase flows is modulated by the chemical pattern on the top and bottom surfaces, leading to a stick-slip behavior of the contact line. The advancing and receding contact angles are equal to the maximum and minimum values of static contact angels of the surfaces respectively. A critical value of the wettability contrast is identified above which the effect of diffusion becomes important, leading to the interesting behavior of fluid-fluid interface breaking, with the transport of the non-wetting fluid being assisted and mediated by rapid diffusion through the wetting fluid. Near the critical value, the time-averaged extra dissipation scales as U, the averaged displacement velocity.

The paper is organized as following. In Section 2, we introduce the stationary two-phase fluid model. We then carry out matched asymptotic analysis for the sharp interface limit in Section 3. In Section 4, we state and prove the Γ-convergence theorem for the sharp interface limit. In Section 5, we consider two explicit examples

and study the stick-slip-jump of the interface and the contact angle hysteresis.

2. The stationary two-phase fluid model. In immiscible two-phase flows, the contact line denotes the intersection of the fluid-fluid interface with the solid wall. It has been shown that the no-slip boundary condition leads to nonphysical contact-line singularity, or infinite viscous dissipation near the moving contact line. Recently, a diffuse-interface model with generalized Navier boundary condition was proposed in [21] to describe the interface motion on solid surface, which involves a coupled system of the Navier-Stokes (NS) equation for the velocity field $\mathbf{u}$ in the presence of the capillary force density and the Cahn-Hilliard (CH) equation for the phase field ϕ

$$\begin{cases} \mathbf{u}_t + (\mathbf{u}\cdot\nabla)\mathbf{u} = -\nabla p + \nu\Delta\mathbf{u} + B\mu\nabla\phi, \\ \phi_t + \mathbf{u}\cdot\nabla\phi = L_d\Delta\mu, \\ \mathrm{div}\mathbf{u} = 0, \\ \mu = -\epsilon\Delta\phi + f'(\phi)/\epsilon. \end{cases} \tag{2.1}$$

Here p is the pressure, μ is the chemical potential, and $f(\phi)$ is the bulk free energy density. ν, B, L_d are physical parameters, and ϵ is a small parameter to characterize the width of the interface between the two fluids. In general, $f(\cdot)$ is a double well function. For simplicity, we choose it as $f(\phi) = \frac{(1-\phi^2)^2}{4}$. In this case, the states of $\phi = \pm 1$ represents the two phases of the fluid, respectively.

The boundary conditions at the solid surface are the impermeability conditions $\partial_n\mu = 0$, $v_n = 0$, the relaxational equation for ϕ:

$$\frac{\partial\phi}{\partial t} + u_\tau\partial_\tau\phi = -V_s L(\phi), \tag{2.2}$$

and the *generalized Navier boundary condition*

$$L_s^{-1}u_\tau^{slip} = -\partial_n u_\tau + B\epsilon^{-1}L(\phi)\partial_\tau\phi. \tag{2.3}$$

Here τ denotes the direction tangent to the solid surface (for two-dimensional flows), n denotes the outward surface normal, V_s is a positive phenomenological parameter, $L(\phi) = \epsilon\partial_n\phi + \partial\gamma(\mathbf{x},\phi)/\partial\phi$ with $\gamma(\mathbf{x},\phi)$ being the fluid-solid interfacial free energy per unit area, L_s is the slip length, and $L(\phi)\partial_\tau\phi$ is the uncompensated Young stress. Notice that $\gamma(\mathbf{x},\phi)$ depends on the position $\mathbf{x}$ on the surface so that it also models the inhomogeneous boundaries.

It is shown that the continuum calculations based on the new model can quantitatively reproduce MD simulation results [21] which shows that the new model provides an accurate description of fluid-solid interfacial phenomena and it also provides an effective tool for performing simulations of two phase flow on rough surfaces.

To describe the stationary wetting phenomena of the fluid on the solid substrates, we let $\mathbf{u} = 0$ and $\partial_t\phi = 0$. Then the N-S-C-H systems (2.1) is reduced to the following system

$$\begin{cases} -\nabla p + B\mu\nabla\phi = 0, \\ \Delta\mu = 0, \\ \mu = -\epsilon\Delta\phi + f'(\phi)/\epsilon. \end{cases} \tag{2.4}$$

The boundary conditions become

$$\begin{cases} \epsilon\partial_{\mathbf{n}}\phi + \partial_\phi\gamma(\mathbf{x},\phi) = 0, \\ \partial_{\mathbf{n}}\mu = 0. \end{cases} \tag{2.5}$$

The stationary N-S-C-H equations (2.4) and (2.5) could be further simplified. From the equation for chemical potential

$$\begin{cases} \Delta\mu = 0, & \text{in } \Omega; \\ \partial_{\mathbf{n}}\mu = 0. & \text{on } \partial\Omega. \end{cases} \tag{2.6}$$

We have

$$\mu \equiv c, \tag{2.7}$$

with some constant c to be determined. Thus, the equations for ϕ and p are reduced to

$$\begin{cases} -\epsilon\Delta\phi + f'(\phi)/\epsilon = c, & \text{in } \Omega, \\ \epsilon\partial_{\mathbf{n}}\phi + \partial_{\phi}\gamma(\mathbf{x},\phi) = 0, & \text{on } \partial\Omega, \end{cases} \tag{2.8}$$

and

$$-\nabla p + B\, c\nabla\phi = 0, \quad \text{in } \Omega. \tag{2.9}$$

This is the phase field model to be studied in this paper.

We remark that the equation (2.8) is the Euler-Lagrange equation of the following constraint functional minimizing problem,

$$\begin{aligned} &\min I_\epsilon(\phi) = \int_\Omega \frac{\epsilon}{2}|\nabla\phi|^2 + \frac{f(\phi)}{\epsilon}dxdy + \int_{\partial\Omega}\gamma(\mathbf{x},\phi)ds, \\ &s.t. \int_\Omega \phi = C_0, \end{aligned} \tag{2.10}$$

with some given constant C_0 such that $-|\Omega| < C_0 < |\Omega|$. The constant c in (2.8) is the Lagrange multiplier for the constrained minimization problem.

3. Sharp interface limit from matched asymptotic expansion. In this section, we will study the behavior of the equations (2.8) and (2.9) when the interface width parameter $\epsilon \to 0$. We use the matched asymptotic expansion method, which has been successfully used in many related free-interface problems (see for example[20][25]). Here we consider the case when the fluid-fluid interface intersects with a flat but chemically patterned surfaces. The results obtained by asymptotic analysis will be proved in the next section. From now on, we will use the notation ϕ^ϵ, p^ϵ and c_ϵ to indicate the explicit dependence of the respective quantities on the small parameter ϵ.

We assume that the interface is given by the zero level set $\Gamma^\epsilon = \{\mathbf{x} \in \bar{\Omega} \mid \phi^\epsilon(\mathbf{x}) = 0\}$. Let $d^\epsilon(\mathbf{x})$ be the signed distance from the point $\mathbf{x} \in \Omega$ in the neighborhood of Γ^ϵ to the interface. The signed distance is such that $|\nabla d^\epsilon| = 1$. Suppose that the $d^\epsilon(\mathbf{x})$ has the expansion that

$$d^\epsilon(\mathbf{x}) = \sum_{j\geq 0} \epsilon^j d_j(\mathbf{x}),$$

then we have $d_0(\mathbf{x})$ is the leading order spatial signed distance from the point $\mathbf{x} \in \Omega^\pm = \{\mathbf{x} \in \bar{\Omega} | \pm d^0(\mathbf{x}) > 0\}$ to $\Gamma^0 = \{\mathbf{x} \in \bar{\Omega} \mid d_0(\mathbf{x}) = 0\}$ and $|\nabla d_0| = 1$. The matched asymptotic analysis is based on an outer expansion away from Γ^0 and an inner expansion in the vicinity of Γ^0.

3.1. The analysis away from the solid boundary. We first study the asymptotic behavior of the solutions away from the solid surface. The analysis in this subsection is standard [4][5].

The outer expansions. We consider the following expansions on ϵ,

$$\phi^\epsilon(\mathbf{x}) = \phi_0(\mathbf{x}) + \epsilon\phi_1(\mathbf{x}) + \epsilon^2\phi_2(\mathbf{x}) + \dots, \tag{3.1}$$

$$p^\epsilon(\mathbf{x}) = p_0(\mathbf{x}) + \epsilon p_1(\mathbf{x}) + \epsilon^2 p_2(\mathbf{x}) + \dots. \tag{3.2}$$

$$c_\epsilon = c_0 + \epsilon c_1 + \epsilon^2 c_2 + \cdots \tag{3.3}$$

We substitute the expansions into the equations $(2.8)_1$ and (2.9). The leading order of the equation $(2.8)_1$ gives

$$f'(\phi_0) = 0.$$

Notice that $f'(\phi) = -\phi + \phi^3$, we have immediately that

$$\phi_0 = \pm 1, \quad \text{in } \Omega^\pm. \tag{3.4}$$

The leading order of (2.9) gives that

$$-\nabla p_0 + B\, c_0 \nabla\phi_0 = 0, \quad \text{in } \Omega^\pm.$$

This implies that $\nabla p_0 = 0$ in Ω^+ and Ω^-, or equivalently

$$p_0 = p_0^\pm, \quad \text{in } \Omega^\pm, \tag{3.5}$$

with two constants p_0^+ and p_0^-.

The inner expansions. Before we do inner expansions, we first define

$$\mathbf{m} = \nabla d_0(\mathbf{x}), \kappa = \Delta d_0(\mathbf{x}). \tag{3.6}$$

When $\mathbf{x} \in \Gamma^0$, $\mathbf{m}$ is the unit normal to Γ^0 pointing toward Ω^+ and κ is the signed mean curvature of Γ^0 at $\mathbf{x}$, which is positive when the center of the curvature lies in Ω^-. We introduce the inner variable in the vicinity of Γ^0,

$$\xi = d^0(\mathbf{x})/\epsilon.$$

Then we suppose that near Γ^0, ϕ^ϵ and p^ϵ could be written in $(\mathbf{x}, \xi)$ as

$$\phi^\epsilon(\mathbf{x}) = \tilde{\phi}(\mathbf{x}, \xi),\ p^\epsilon(\mathbf{x}) = \tilde{p}(\mathbf{x}, \xi).$$

It is easy to see that

$$\left.\begin{array}{l} \nabla = \nabla_{\mathbf{x}} + \epsilon^{-1}\mathbf{m}\partial_\xi, \\ \Delta = \Delta_{\mathbf{x}} + \epsilon^{-1}\kappa\partial_\xi + \epsilon^{-2}\partial_{\xi\xi}. \end{array}\right\} \tag{3.7}$$

Thus, the equations $(2.8)_1$ and (2.9) could be rewritten as

$$-\epsilon^{-1}\partial_{\xi\xi}\tilde{\phi} - \kappa\partial_\xi\tilde{\phi} - \epsilon\Delta_{\mathbf{x}}\tilde{\phi} + \epsilon^{-1}(-\tilde{\phi} + \tilde{\phi}^3) = c_\epsilon, \quad \text{in } \Omega; \tag{3.8}$$

and

$$\nabla_{\mathbf{x}}(-\tilde{p} + Bc_\epsilon\tilde{\phi}) + \epsilon^{-1}\mathbf{m}\partial_\xi(-\tilde{p} + Bc_\epsilon\tilde{\phi}) = 0, \quad \text{in } \Omega. \tag{3.9}$$

Now we suppose the following expansions of $\tilde{\phi}$ and $\tilde{p}$,

$$\tilde{\phi}(\mathbf{x},\xi) = \tilde{\phi}_0(\mathbf{x},\xi) + \epsilon\tilde{\phi}_1(\mathbf{x},\xi) + \epsilon^2\tilde{\phi}_2(\mathbf{x},\xi) + \cdots, \tag{3.10}$$

$$\tilde{p}(\mathbf{x},\xi) = \tilde{p}_0(\mathbf{x},\xi) + \epsilon\tilde{p}_1(\mathbf{x},\xi) + \epsilon^2\tilde{p}_2(\mathbf{x},\xi) + \cdots. \tag{3.11}$$

We substitute these expansions into (3.8) and (3.9). Then we have, for the leading order

$$-\partial_{\xi\xi}\tilde{\phi}_0 + (-\tilde{\phi}_0 + \tilde{\phi}_0^3) = 0, \tag{3.12}$$

and

$$\partial_\xi\tilde{p}_0 - Bc_0\partial_\xi\tilde{\phi}_0 = 0. \tag{3.13}$$

In the next order, we have

$$-\kappa\partial_\xi\tilde{\phi}_0 + (-\partial_{\xi\xi}\tilde{\phi}_1 - \tilde{\phi}_1 + 3\tilde{\phi}_0^2\tilde{\phi}_1) = c_0. \tag{3.14}$$

Matching the inner and outer expansions. We require the following matching conditions

$$\sum_{j\geq 0}\epsilon^j\tilde{\phi}_j(\mathbf{x},\xi) \approx \sum_{j\geq 0}\epsilon^j\phi_j(\mathbf{x}),$$

$$\sum_{j\geq 0}\epsilon^j\tilde{p}_j(\mathbf{x},\xi) \approx \sum_{j\geq 0}\epsilon^j p_j(\mathbf{x}),$$

for $\xi = \frac{d^0(\mathbf{x})}{\epsilon}$ near Γ^0. Therefore, we have

$$\lim_{\xi\to\pm\infty}\tilde{\phi}_0 = \phi_0^{\pm} = \pm 1, \lim_{\xi\to\pm\infty}\tilde{p}_0 = p_0^{\pm}. \tag{3.15}$$

Combine with (3.12) and $\tilde{\phi}_0(\mathbf{x},0) = 0$, we could conclude that

$$\tilde{\phi}_0(\mathbf{x},\xi) = \Phi(\xi), \qquad \forall\mathbf{x}\in\Gamma^0\cap\Omega, \tag{3.16}$$

where Φ is the unique solution of the following ordinary differential equation,

$$\begin{cases} -\Phi''(\xi) - \Phi(\xi) + \Phi(\xi)^3 = 0, \quad -\infty < \xi < +\infty \\ \lim_{\xi\to\pm\infty}\Phi = \pm 1, \Phi(0) = 0. \end{cases} \tag{3.17}$$

Then from the equation (3.14), $\tilde{\phi}_1$ is such that

$$-\partial_{\xi\xi}\tilde{\phi}_1 - \tilde{\phi}_1 + 3\Phi^2\tilde{\phi}_1 = c_0 + \kappa\Phi'. \tag{3.18}$$

We multiply the equation by Φ' and integrate in ξ from $(-\infty,+\infty)$. The left-hand side then vanishes and we obtain

$$2c_0 + \kappa\int_{-\infty}^{\infty}(\Phi')^2 d\xi = 0.$$

Denote the constant $\sigma = \int_{-\infty}^{\infty}(\Phi')^2 d\xi$, which represents the interface tension[4]. We are led to

$$\kappa = -2c_0/\sigma. \tag{3.19}$$

Therefore the curvature is a constant.

Furthermore, we integrate (3.13) in ξ from $-\infty$ to $+\infty$, and we have

$$[p_0] = 2Bc_0 = -B\sigma\kappa \tag{3.20}$$

where $[p_0] = p_0^+ - p_0^-$ is the jump of pressure on the interface Γ^0. This is exactly the Laplace formula in fluid dynamics.

3.2. The analysis on the solid boundaries. We now study the asymptotic behavior of Equation (2.8) on the solid boundaries. We first consider the outer expansion away from the contact point. Substitute the expansion (3.1) into the equation $(2.8)_2$, the leading order then leads to

$$\partial_\phi \gamma(\mathbf{x}, \phi_0) = 0, \quad \text{on } \partial\Omega \cap \Omega^{\pm}.$$

Notice that $\phi_0 = \pm 1$ in the field $\Omega^{\pm}$, respectively. So we have

$$\partial_\phi \gamma(\mathbf{x}, 1) = 0, \quad \mathbf{x} \in \partial\Omega \cap \Omega^{+}, \tag{3.21}$$

$$\partial_\phi \gamma(\mathbf{x}, -1) = 0, \quad \mathbf{x} \in \partial\Omega \cap \Omega^{-}. \tag{3.22}$$

We then consider the inner expansion near the contact point on the solid boundary.

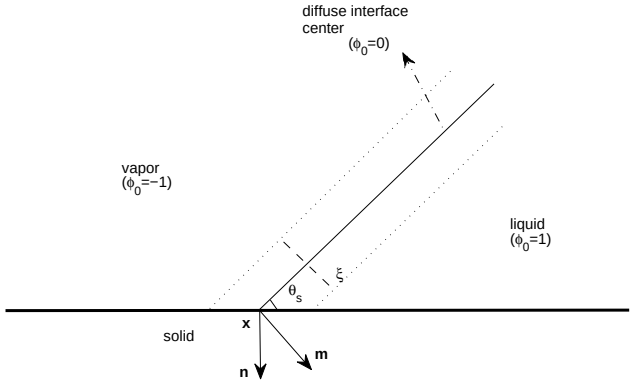

FIG. 3.1. *The inner expansion on the solid surfaces.*

Using the local coordinate ξ defined in the last subsection, equation $(2.8)_2$ then reads

$$\epsilon \mathbf{n} \cdot (\nabla_{\mathbf{x}} + \epsilon^{-1}\mathbf{m})\partial_\xi \tilde{\phi} + \partial_\phi \gamma(\mathbf{x}, \tilde{\phi}) = 0, \qquad \text{on } \partial\Omega. \tag{3.23}$$

Here $\mathbf{n}$ is the out unit normal of the boundary $\partial\Omega$, and $\mathbf{m}$ is the unit normal of the interface Γ pointing into Ω^+(see Figure 3.1). Then we substitute the inner expansion (3.10) into the equation and take the leading order, we have

$$\mathbf{n} \cdot \mathbf{m}\partial_\xi \tilde{\phi}_0 + \partial_\phi \gamma(\mathbf{x}, \tilde{\phi}_0) = 0, \qquad \text{on } \partial\Omega. \tag{3.24}$$

We suppose that the formula (3.16) on $\tilde{\phi}_0$ could be extended directly to the boundary $\partial\Omega$ by keeping the values invariant along the tangential direction of the interface Γ(as shown in Figure 3.1). Then from the above equation, we know that

$$\mathbf{n} \cdot \mathbf{m}\Phi' + \partial_\phi \gamma(\mathbf{x}, \Phi) = 0,$$

for the contact point $\mathbf{x} \in \Gamma \cap \partial\Omega$. Here Φ is given by (3.17).

We assume that the two domains $\Omega^{\pm}$ where $\phi_0 = +1$ and $\phi_0 = -1$ represent the liquid phase and the vapor phase, respectively. It is easy to see that $\mathbf{n} \cdot \mathbf{m} = \cos\theta_s$, with θ_s is the static contact angle of the liquid phase($\phi_0 = 1$) on the solid boundary. So the above equation could be rewritten as

$$\Phi' \cos\theta_s + \partial_\phi \gamma(\mathbf{x}, \Phi) = 0. \tag{3.25}$$

The chemically homogeneous surface When the solid interface is homogeneous, i.e., $\gamma(\mathbf{x}, \Phi)$ is independent of $\mathbf{x}$ and $\gamma(\mathbf{x}, \Phi) = \gamma(\Phi)$. Then we multiply the equation (3.25) by Φ' and integrate in ξ from $-\infty$ to $+\infty$, we have

$$\int_{-\infty}^{+\infty} (\Phi')^2 d\xi \cos\theta_s + \int_{-\infty}^{+\infty} \gamma'(\Phi)\Phi' d\xi = 0,$$

or equivalently,

$$\int_{-\infty}^{+\infty} (\Phi')^2 d\xi \cos\theta_s + \int_{-1}^{1} \gamma'(\Phi) d\Phi = 0.$$

This gives

$$\sigma \cos\theta_s + (\gamma(1) - \gamma(-1)) = 0, \tag{3.26}$$

with $\sigma = \int_{-\infty}^{+\infty} (\Phi')^2 d\xi$ being the surface tension. We denote $\gamma_{SV} = \gamma(-1)$ and $\gamma_{SL} = \gamma(1)$, which represent the solid-vapor and solid-liquid surface energy density, respectively. Then the above equation is

$$\cos\theta_s = \frac{\gamma_{SV} - \gamma_{SL}}{\sigma}. \tag{3.27}$$

which is the so-called Young's equation on wetting contact angles.

For simplicity, we assume that $\gamma(\phi)$ be a function interpolating $\gamma_{SV} = \gamma(-1)$ and $\gamma_{SL} = \gamma(1)$ in the form of $\gamma(\phi) = \frac{\gamma_{SV}+\gamma_{SL}}{2} - \frac{\gamma_{SV}-\gamma_{SL}}{4}(3\phi - \phi^3)$ (this is the unique formula for the equation (3.25) to be exactly correct on a planar surface[28, 30]). Then from the Young's equation (3.27), we have

$$\gamma'(\phi) = -\frac{\sigma}{2} \cos\theta_s s_\gamma(\phi), \tag{3.28}$$

with $s_\gamma = \frac{3}{2}(1 - \phi^2)$. It is easy to see that such a formula for $\gamma'(\phi)$ satisfies the equations (3.21) and (3.22).

The chemically patterned surface. We assume that the solid boundary is periodically patterned with two parts $\mathcal{A}$ and $\mathcal{B}$ with different surface energy densities $\gamma_{\mathcal{A}}(\phi)$ and $\gamma_{\mathcal{B}}(\phi)$ such that

$$\gamma'_{\mathcal{A}}(\phi) = -\frac{\sigma}{2} \cos\theta_{\mathcal{A}} s_\gamma(\phi),\ \gamma'_{\mathcal{B}}(\phi) = -\frac{\sigma}{2} \cos\theta_{\mathcal{B}} s_\gamma(\phi),$$

with different angles $\theta_{\mathcal{A}}$ and $\theta_{\mathcal{B}}$. We then define the surface energy density $\gamma(\mathbf{x}, \phi)$ on each period as

$$\gamma(\mathbf{x}, \phi) = \begin{cases} \gamma_{\mathcal{A}}(\phi), & \mathbf{x} \in \mathcal{A}; \\ \gamma_{\mathcal{B}}(\phi), & \mathbf{x} \in \mathcal{B}. \end{cases} \tag{3.29}$$

Here $\mathcal{A}$ and $\mathcal{B}$ are disjoint open sets. We denotes $\mathcal{R}$ as the set of discrete border points between $\mathcal{A}$ and $\mathcal{B}$.

Let $\tilde{\mathbf{x}}_0$ be a contact point (the intersection of the interface with the boundary). Similar to the derivation for the chemically homogeneous boundary, when $\tilde{\mathbf{x}}_0 \in \mathcal{A}$, we have

$$\theta_s = \theta_{\mathcal{A}},$$

and when $\tilde{\mathbf{x}}_0 \in \mathcal{B}$, we have

$$\theta_s = \theta_{\mathcal{B}}.$$

The situation is more complicated when the contact point $\tilde{\mathbf{x}}_0$ is the common boundary point $\mathbf{x}_0$ defined above since the surface energy density function $\gamma(\mathbf{x}, \phi)$ is discontinuous at $\mathbf{x}_0$. To perform the asymptotic analysis in this case, we smooth out $\gamma(\mathbf{x}, \phi)$ as follows:

$$\gamma^\delta(\mathbf{x}, \phi) = \begin{cases} \gamma_{\mathcal{A}}(\phi), & s(\mathbf{x}, \mathbf{x}_0) < -\frac{\delta}{2}; \\ \gamma_{\mathcal{B}}(\phi), & s(\mathbf{x}, \mathbf{x}_0) > \frac{\delta}{2}; \\ \left(\frac{1}{2} + \frac{s(\mathbf{x},\mathbf{x}_0)}{\delta}\right)\gamma_{\mathcal{A}}(\phi) + \left(\frac{1}{2} - \frac{s(\mathbf{x},\mathbf{x}_0)}{\delta}\right)\gamma_{\mathcal{B}}(\phi), & -\frac{\delta}{2} \le s(\mathbf{x}, \mathbf{x}_0) \le \frac{\delta}{2}. \end{cases}$$

Here $s(\mathbf{x}, \mathbf{x}_0)$ is the signed distance from $\mathbf{x}$ to $\mathbf{x}_0$ along the solid boundary and $\delta > 0$ is a small parameter. We now assume that the contact point $\tilde{\mathbf{x}}_0$ is in the small neighborhood of $\mathbf{x}_0$ such that $-\frac{\delta}{2} \le s(\tilde{\mathbf{x}}_0, \mathbf{x}_0) \le \frac{\delta}{2}$. Then from the equation (3.25), we have

$$\int_{-\infty}^{+\infty} (\Phi')^2 d\xi \cos\theta_s + \lambda \int_{-\infty}^{+\infty} \gamma'_{\mathcal{A}}(\Phi)\Phi' d\xi + (1-\lambda) \int_{-\infty}^{+\infty} \gamma'_{\mathcal{B}}(\Phi)\Phi' d\xi = 0.$$

where $\lambda = \frac{1}{2} + \frac{s(\tilde{\mathbf{x}_0},\mathbf{x}_0)}{\delta} \in [0, 1]$. This implies the contact angle on $\tilde{\mathbf{x}}_0$ is such that

$$\cos\theta_s = \lambda \cos\theta_{\mathcal{A}} + (1-\lambda)\cos\theta_{\mathcal{B}}.$$

Then let $\delta \to 0$, $s(\tilde{\mathbf{x}}_0, \mathbf{x}_0) \to 0$ while $s(\tilde{\mathbf{x}}_0, \mathbf{x}_0)/\delta$ is kept fixed. We get the contact angle on $\mathbf{x}_0$ could be given by

$$\cos\theta_s = \lambda \cos\theta_{\mathcal{A}} + (1-\lambda)\cos\theta_{\mathcal{B}}. \tag{3.30}$$

Notice that λ can take any value between 0 and 1 under various choice of $\tilde{\mathbf{x}}_0$ in above analysis. Therefore, when the contact point is exactly the meeting point between $\mathcal{A}$ and $\mathcal{B}$, the contact angle θ_s is not unique and can take any value in the range $\theta_{\mathcal{A}} \le \theta_s \le \theta_{\mathcal{B}}$. The exact value of θ_s has to be determined by other conditions. In the above analysis, it depends on how $\tilde{\mathbf{x}}_0$ approaches $\mathbf{x_0}$.

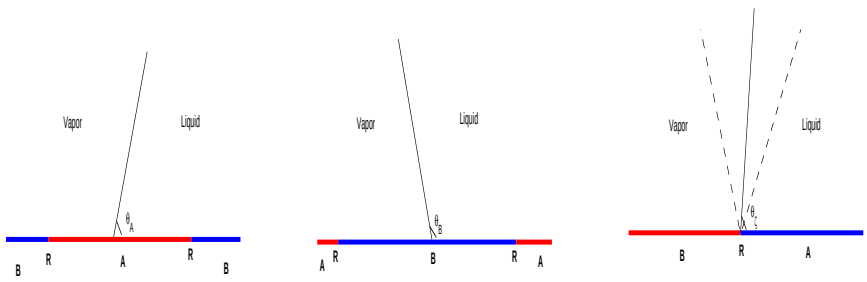

(a) The contact point on $\mathcal{A}$ (b) The contact point on $\mathcal{B}$ (c) The contact point at $\mathcal{R}$

FIG. 3.2. *The contact angles on chemically patterned surface.*

In conclusion, on the chemically patterned surface, we have that the contact angle at the contact point $\tilde{\mathbf{x}}_0$ in various situations as (see Figure 3.2)

$$\theta_s = \begin{cases} \theta_{\mathcal{A}}, & \text{if } \tilde{\mathbf{x}}_0 \in \mathcal{A}; \\ \theta_{\mathcal{B}}, & \text{if } \tilde{\mathbf{x}}_0 \in \mathcal{B}; \\ \theta_{\zeta}, & \text{if } \tilde{\mathbf{x}}_0 \in \mathcal{R}; \end{cases} \tag{3.31}$$

with some θ_ζ such that $\theta_{\mathcal{A}} \le \theta_\zeta \le \theta_{\mathcal{B}}$. At the borders of the patterned strips, the value of the contact angle is not unique and has to be determined by additional physical conditions.

4. Analysis of the variational problem. The results by asymptotic analysis in last section will be proved in this section. It is easy to see that the stationary problem (2.8) is equivalent to the following energy minimizing problem.

$$\min I_\epsilon(\phi^\epsilon) = \begin{cases} \int_\Omega \frac{\epsilon}{2}|\nabla\phi^\epsilon|^2 + \frac{f(\phi^\epsilon)}{\epsilon}dxdy + \int_{\partial\Omega}\gamma(\mathbf{x},\phi^\epsilon)ds, & \text{if } \int_\Omega \phi^\epsilon = C_0; \\ +\infty, & \text{otherwise.} \end{cases} \tag{4.1}$$

with some fixed constant $-|\Omega| < C_0 < |\Omega|$. Thus, to understand the behavior of the stable solution of (2.8), it is equivalent to study the minimizers of the problem (4.1).

4.1. Preliminary. The convergence of functional minimizing problems could be illustrated through Γ-convergence theory[3, 8]. In this subsection, we introduce some general definitions and results on Γ-convergence. The following definition of Γ-convergence is given in [3].

DEFINITION 4.1. *Let U be a metric space equipped with the distance ρ. We say a sequence of functionals $F_j : U \to \mathbb{R} \cup \{\infty\}$* Γ-converges *to $F_0 : U \to \mathbb{R} \cup \{\infty\}$ if for all $u \in U$ we have*

(i) (lower bound inequality) for every sequence u_j converging to u

$$F_0(u) \le \liminf_{j\to\infty} F_j(u_j);$$

(ii) (upper bound inequality) there exists a sequence u_j converging to u such that

$$F_0(u) \ge \limsup_{j\to\infty} F_j(u_j).$$

We then introduce some definitions on local minimizers([15]). We say u is a *local minimizer* of a functional F, if

$$F(u) \le F(v), \qquad \text{whenever } \rho(u,v) < \delta$$

for some $\delta > 0$. u is called an *isolated local minimizer* of the functional F, if

$$F(u) < F(v), \qquad \text{whenever } 0 < \rho(u,v) < \delta$$

for some $\delta > 0$. Specifically, we say u is a *L_1-local minimizer* (an *isolated L_1-local minimizer*) if the distance ρ in above definitions is given by $\rho(u,v) = \|u - v\|_{L^1(\Omega)}$.

To study the convergence behavior of minimizers based on Γ-convergence theory, we need more restrictions on the functionals. A functional F is said to be *lower semicontinuous*, if for any $u \in U$ and any sequence u_j converging to u, we have

$$F(u) \le \liminf_{j\to\infty} F(u_j).$$

A sequence of functionals F_j are said to be *equicoercive*, if for any sequence u_j such that $\sup_j F_j(u_j) < \infty$, there exists a subsequence of u_j converging to some $u \in U$.

The following lemma is given by R. V. Kohn and P. Sternberg[15].

LEMMA 4.1. *Let (U, ρ) be a complete metric space and consider a sequence of functionals $F_j : U \to \mathbb{R} \cup \{\infty\}$. Suppose that they are equicoercive and lower semi-continuous. Suppose also that the sequence F_j Γ-converges to F_0 as $j \to \infty$. If u_0 is a isolated local minimizer of F_0, then there is a sequence $\{u_j\}$ of local minimizers of F_j, such that $\rho(u_j, u_0) \to 0$ as $j \to \infty$.*

4.2. The Γ-convergence result. We now study the limiting behavior of the problem (4.1) as ϵ goes to 0. A similar problem with chemically homogeneous boundary has been analyzed by L. Modica[17]. The following proposition is a direct generalization of the result in [17].

PROPOSITION 4.1. *In the bounded variational function space $BV(\Omega)$, the functional I_ϵ Γ-converges to $\tilde{I}_0$ in $L^1(\Omega)$ sense as ϵ goes to 0, with $\tilde{I}_0$ being defined as*

$$\tilde{I}_0(\phi) = \begin{cases} \tilde{\sigma}|\partial\Omega_1 \cap \Omega| + \int_{\partial\Omega_1 \cap \partial\Omega} \tilde{\gamma}(\mathbf{x}, 1)ds + \int_{\partial\Omega \setminus \partial\Omega_1} \tilde{\gamma}(\mathbf{x}, -1)ds, & \text{if } \phi(x) = \pm 1, \text{ a.e.} \\ & \quad \text{and } \int_\Omega \phi = C_0; \\ +\infty, & \text{otherwise.} \end{cases}$$

Here $\Omega_1 = \{\mathbf{x} \in \Omega : \phi(\mathbf{x}) = 1\}$, the surface energy density is

$$\tilde{\gamma}(\mathbf{x}, t) = \inf_s \big\{\gamma(\mathbf{x}, s) + \big| \int_s^t \big(2f(r)\big)^{1/2} dr\big|\big\},$$

and interface energy density is

$$\tilde{\sigma} = \int_{-1}^{1} \big(2f(r)\big)^{1/2} dr.$$

REMARK 4.1. *The difference of the above result from that of Modica[17] is that we allow an inhomogeneous boundary energy density $\gamma(\mathbf{x}, \phi)$. The proof of the proposition is similar to that of Theorem 2.1 in [17] and is given in the Appendix.*

For a specific choice of the bulk free energy density $f(\phi) = \frac{(1-\phi^2)^2}{4}$, we have the following proposition.

PROPOSITION 4.2. *In the bounded variational function space $BV(\Omega)$, the functional I_ϵ Γ-converges to I_0 in $L^1(\Omega)$ sense as ϵ goes to 0, with I_0 being defined as*

$$I_0(\phi) = \begin{cases} \sigma|\partial\Omega_1 \cap \Omega| + \int_{\partial\Omega_1 \cap \partial\Omega} \gamma(\mathbf{x}, 1)ds + \int_{\partial\Omega \setminus \partial\Omega_1} \gamma(\mathbf{x}, -1)ds, & \text{if } \phi(x) = \pm 1 \text{ a.e.} \\ & \quad \text{and } \int_\Omega \phi = C_0; \\ +\infty, & \text{otherwise.} \end{cases} \tag{4.2}$$

Here $\Omega_1 = \{x \in \Omega : \phi(x) = 1\}$, and the interface energy density is given by

$$\sigma = \int_{-\infty}^{+\infty} (\Phi')^2 d\xi,$$

with $\Phi(\xi)$ defined by (3.17).

Proof. We only need to show that I_0 is the same as $\tilde{I}_0$ under the special choice of $f(\phi) = \frac{(1-\phi^2)^2}{4}$.

First, we show that $\sigma = \tilde{\sigma}$. Notice that from (3.17), we have

$$\Phi''(\xi) = f'(\Phi).$$

Multiplying by Φ' we get,

$$\frac{d}{d\xi}\frac{\Phi'^2}{2} = \frac{d}{d\xi} f(\Phi(\xi)).$$

From the boundary conditions that $\Phi \to \pm 1$ and $\Phi' \to 0$ as $\xi \to \pm\infty$, we have

$$\frac{\Phi'^2}{2} = f(\Phi(\xi)).$$

Since f is a nonnegative function, and Φ is a monotonic increasing function, we have $\Phi' = (2f(\Phi))^{1/2}$ and

$$\sigma = \int_{-\infty}^{\infty} (\Phi')^2 d\xi = \int_{-\infty}^{\infty} (2f(\Phi))^{1/2}\Phi' d\xi = \int_{-1}^{1} (2f(\Phi))^{1/2} d\Phi = \tilde{\sigma}. \tag{4.3}$$

In addition, we could compute that

$$\sigma = \tilde{\sigma} = \frac{1}{\sqrt{2}}\int_{-1}^{1}(1-r^2)dr = \frac{2\sqrt{2}}{3}.$$

Now we consider the value $\tilde{\gamma}(\mathbf{x}, \pm 1)$. We need the exact form of $\gamma(\mathbf{x}, s)$. From (3.28), we have

$$\gamma(\mathbf{x}, s) = C - \frac{\sigma}{4}\cos\theta(\mathbf{x})(3s - s^3) = C - \frac{\sqrt{2}}{6}\cos\theta(\mathbf{x})(3s - s^3).$$

for some constant C, which is independent on s. Then we could get, for $-1 \le s, t \le 1$,

$$\begin{aligned} F(\mathbf{x}, t, s) &= \gamma(\mathbf{x}, s) + \frac{\sqrt{2}}{2}\Big|\int_s^t \big(2f(r)\big)^{1/2} dr\Big| \\ &= C - \frac{\sqrt{2}}{6}\cos\theta(\mathbf{x})(3s - s^3) + \frac{\sqrt{2}}{2}\Big|\int_s^t (1-r^2)dr\Big|, \end{aligned}$$

Direct computation shows that

$$\tilde{\gamma}(\mathbf{x}, 1) = \min_s F(\mathbf{x}, 1, s) = F(\mathbf{x}, 1, 1) = \gamma(\mathbf{x}, 1), \tag{4.4}$$

and aslo

$$\tilde{\gamma}(\mathbf{x}, -1) = \min_s F(\mathbf{x}, -1, s) = F(\mathbf{x}, -1, -1) = \gamma(\mathbf{x}, -1). \tag{4.5}$$

This completes the proof. □

4.3. The convergence of the minimizers. Using Lemma 4.1 and Proposition 4.2, we can prove the following theorem,

THEOREM 4.1. *If $\phi_0 \in BV(\Omega)$ is the isolated L^1-local minimizer of I_0, then there exists a sequence $\phi_{\epsilon_j} \in BV(\Omega)$ of the L^1-local minimizers of I_{ϵ_j}, such that*

$$\lim_{j\to\infty} \|\phi_{\epsilon_j} - \phi_0\|_{L^1} = 0.$$

as $\epsilon_j \to 0$.

Proof. We only need to show the lower semicontinuous and equicoercive of the functional I_ϵ in L^1 norm. The proof of the theorem is then standard.

First, we prove the lower semicontinuity. For some $\phi_\infty \in BV(\Omega)$, suppose a sequence $\phi_j \in H^1(\Omega)$ converge to ϕ_∞ in $L^1(\Omega)$, we would like to show that

$$I_\epsilon(\phi_\infty) \leq \liminf_{j\to\infty} I_\epsilon(\phi_j). \tag{4.6}$$

Without loss of generality, we assume that there exists a constant M_1 such that

$$\lim_{j\to\infty} I_\epsilon(\phi_j) = M_1 < \infty.$$

Since $f(\cdot) \geq 0$ and $\gamma(\cdot,\cdot) \geq 0$, then we could know that $|\phi_j|_{H^1(\Omega)} < M_1/\epsilon$. Thus, there exists a subsequence of ϕ_j, without loss of generality, still denoted by ϕ_j, such that

$$\phi_j \rightharpoonup \phi_\infty \text{ in } H^1(\Omega), \text{ and } \phi_j(\mathbf{x}) \to \phi_\infty(\mathbf{x}), a.e. \mathbf{x} \in \Omega.$$

Then, applying Fatou's lemma, (4.6) can be obtained by the weakly lower semicontinuity of the functional $\epsilon \int_\Omega |\nabla\phi|^2 dx$ (see [12]) and the continuity of $f(\cdot)$ and $\gamma(\mathbf{x},\cdot)$.

Next, we show the equicoercivity of I_ϵ. We need to prove that, for any sequences $\epsilon_j \to 0$ and ϕ_j such that $\sup_j I_{\epsilon_j}(\phi_j) < \infty$, there exists a subsequence of ϕ_j converging to some function ϕ in L^1 norm.

We suppose that there exists a constant M_2 such that $I_{\epsilon_j}(\phi_j) < M_2$, then we have

$$\int_\Omega \frac{(1-\phi_j^2)^2}{4} dx = \int_\Omega f(\phi_j) dx < M_2\epsilon_j \to 0, \quad \text{as } j \to \infty.$$

This implies that there exists a subsequence of ϕ_j, without loss of generality, still denoted by ϕ_j, converges in measure to some piecewise constant function ϕ. It is also easy to see that ϕ_j are uniformly bounded in L^∞, and hence from the convergence in measure, we have, up to a subsequence, ϕ_j converge to the function ϕ in L^1 norm. ∎

4.4. The properties of the limiting minimizers. Now we study the geometric properties of the minimizers for the limiting functional I_0 in (4.2). The following theorem is a generalization of the results by X. Chen and M.Kowalczyk[7].

We assume that the patterned boundary $\partial\Omega = \mathcal{A}\cup\mathcal{B}\cup\mathcal{R}$, with $\mathcal{A}$ and $\mathcal{B}$ being two disjoint open subsets of $\partial\Omega$, $\mathcal{R} = \{\mathbf{x}_i\}$ composed by some discrete points, we suppose the surface energy density function is defined as

$$\gamma(\mathbf{x},\phi) = \begin{cases} \gamma_{\mathcal{A}}(\phi), & \mathbf{x} \in \mathcal{A}; \\ \gamma_{\mathcal{B}}(\phi), & \mathbf{x} \in \mathcal{B}. \end{cases}$$

Here $\gamma_{\mathcal{A}}(\phi)$ and $\gamma_{\mathcal{B}}(\phi)$ are such that

$$\gamma'_{\mathcal{A}}(\phi) = -\frac{\sigma}{2}\cos\theta_{\mathcal{A}} s_\gamma(\phi), \ \gamma'_{\mathcal{B}}(\phi) = -\frac{\sigma}{2}\cos\theta_{\mathcal{B}} s_\gamma(\phi),$$

with $s_\gamma(\phi) = \frac{3}{2}(1-\phi^2)$. Without loss of generality, we assume that $0 < \theta_{\mathcal{A}} < \theta_{\mathcal{B}} < \pi$.

THEOREM 4.2. *Let* $\phi_0 \in BV(\Omega)$ *be a* L^1*-local minimizer of* I_0*. Then, we have*

- $\phi_0(\mathbf{x}) = \pm 1, a.e. \mathbf{x} \in \Omega$*;*

- *the interface* $\Gamma = \partial\Omega_1 \cap \Omega$*, with* $\Omega_1 = \{\mathbf{x} \in \Omega : \phi_0(\mathbf{x}) = 1\}$*, is of constant curvature;*
- *the contact angle of the phase* ($\phi_0 = 1$) *at some contact point* $\mathbf{x}_0$ *is*

$$\theta_s = \begin{cases} \theta_{\mathcal{A}}, & \text{if } \mathbf{x}_0 \in \mathcal{A}; \\ \theta_{\mathcal{B}}, & \text{if } \mathbf{x}_0 \in \mathcal{B}; \\ \theta_{\zeta}, & \text{if } \mathbf{x}_0 \in \mathcal{R}; \end{cases} \tag{4.7}$$

with some θ_ζ *such that* $\theta_{\mathcal{A}} \le \theta_\zeta \le \theta_{\mathcal{B}}$.

Proof. We firstly prove that the interface $\Gamma = \partial\Omega_1 \cap \Omega$ is of constant curvature. For simplicity, we suppose that $|\Omega_1|$ is samll, and Γ is composed of a simple connected curve, which intersects with $\partial\Omega$ on two points $\mathbf{x}_1$ and $\mathbf{x}_2$.

Suppose that the curvature of Γ is not constant. Then there exists a domain $\Omega_2 \subset \Omega$, such that $|\Omega_2| = |\Omega_1|$, $\tilde{\Gamma} = \partial\Omega_2 \cap \Omega$ is a circular arc that intersects with $\partial\Omega$ at the two points $\mathbf{x}_1$ and $\mathbf{x}_2$. Then we extend Ω_2 outside of Ω to a full circular disk D. From the geometric fact that a disk has the smallest circumference among all shapes with the same area, we have

$$|\tilde{\Gamma}| < |\Gamma|.$$

This implies that, for $\tilde{\phi} = \chi_{\Omega_2} - \chi_{\Omega\setminus\Omega_2}$, with χ_{Ω_2} and $\chi_{\Omega\setminus\Omega_2}$ being the characteristic function of the domains Ω_2 and $\Omega \setminus \Omega_2$, respectively,

$$I_0(\tilde{\phi}) < I_0(\phi).$$

One can define a homotopic mapping $H(s,\lambda)$, $0 \le \lambda \le 1$, with $H(s,0)$ and $H(s,1)$ representing the curves Γ and $\tilde{\Gamma}$ respectively, such that the length of the curve $H(s,\lambda)$ is strictly monotonic decreasing with respect to λ while the area Ω_λ bounded by the curve $H(s,\lambda)$ and $\partial\Omega$ keeps constant for any λ. Thus, the functions $\phi_\lambda = \chi_{\Omega_\lambda} - \chi_{\Omega\setminus\Omega_\lambda}$ converges to ϕ_0 in L^1 norm when $\lambda \to 0$, and

$$I_0(\phi_\lambda) < I_0(\phi), \qquad 0 < \lambda < 1.$$

This contradicts with the fact that ϕ is a L^1-local minimizer of I_0. Thus, Γ is of constant curvature.

Next, we study the contact angles of the phase $\phi_0(\mathbf{x}) = 1$ with respect to a local minimizer ϕ_0. We follow the procedure used in [7]. We identify the points in Ω with complex numbers. Suppose that $z(\tau) : \mathbb{R}^1 \to \mathbb{C}$ is the counterclockwise oriented arclength parameterization of $\partial\Omega$. Then, $z'(\tau)$ is the tangential direction of $\partial\Omega$ at the point $z(\tau)$. We then define the following complex function

$$w(t,\tau,\kappa,\theta) = z(\tau) + z'(\tau)e^{i\theta}\int_0^t e^{i\kappa\tau}d\tau. \tag{4.8}$$

It is easy to see that $w(\cdot,\tau,\kappa,\theta)$ is an arclength parameterization of circular arc that intersects $\partial\Omega$ at $z(\tau)$, with a contact angle θ and has curvature κ. Here the increasing direction of $w(t,\tau,\kappa,\theta)$ with respect to t indicates the counterclockwise orientation. θ is defined as the angle of the counterclockwise rotation from $z'(\tau)$ to $w_t(0,\tau,\kappa,\theta)$(see figure 4.1). Furthermore, one can show that (see [7]), for any positive constant $0 < A < |\Omega|$, there exists a pair (τ,ς), a positive curvature κ, an angle $\theta \in [0, 2\pi)$ and a constant $L \in (0, 2\pi/|\kappa|)$, such that

$$z(\varsigma) = w(L,\tau,\kappa,\theta), \tag{4.9}$$

$$A = \frac{1}{2}\mathrm{Im}\{\int_0^L \bar{w}(t,\tau,\kappa,\theta)w_t(t,\tau,\kappa,\theta)dt + \int_\varsigma^\tau \bar{z}(t)z'(t)dt\}, \tag{4.10}$$

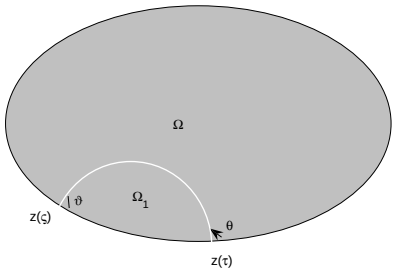

FIG. 4.1. *the definition of θ and ϑ.*

This means that there exists a circular arc which intersects $\partial\Omega$ at $z(\tau)$ and $z(\varsigma)$, with the arc length L and enclosed area A. Here θ, κ, and L are functions of (τ, ς). Furthermore, we have

$$\frac{\partial L}{\partial \tau} = -\cos\theta(\tau,\varsigma), \quad \frac{\partial L}{\partial \varsigma} = -\cos\vartheta(\tau,\varsigma), \tag{4.11}$$

where ϑ is the contact angle of the circular arc at $z(\varsigma)$, defined as the angle of the counterclockwise rotation from $\partial\Omega$ to the arc (see Figure 4.1).

Now we compute the derivative of $I_0(\phi_0)$ with respect to τ and ς. For simplicity, we consider only the derivative in τ. Suppose that the point $z(\tau)$ is in $\mathcal{A}$, then we have

$$\begin{aligned}\frac{\partial I_0}{\partial \tau} &= \sigma\frac{\partial L}{\partial \tau} + \frac{\partial}{\partial \tau}\left(\int_{\partial\Omega_1\cap\partial\Omega}\gamma(\mathbf{x},1)ds\right) + \frac{\partial}{\partial \tau}\left(\int_{\partial\Omega\setminus\partial\Omega_1}\gamma(\mathbf{x},-1)ds\right)\\ &= -\sigma\cos\theta + \gamma_{\mathcal{A}}(1) - \gamma_{\mathcal{A}}(-1).\end{aligned} \tag{4.12}$$

Since ϕ_0 is a local minimizer, we have $\frac{\partial I_0}{\partial \tau} = 0$, which means

$$-\sigma\cos\theta + \gamma_{\mathcal{A}}(1) - \gamma_{\mathcal{A}}(-1) = 0.$$

Notice again that the contact angle of phase ($\phi_0 = 1$) on the point $z(\tau)$ is $\theta_s = \pi - \theta$, we have

$$\cos\theta_s = -\cos\theta = \frac{\gamma_{\mathcal{A}}(-1) - \gamma_{\mathcal{A}}(1)}{\sigma} = \cos\theta_{\mathcal{A}}. \tag{4.13}$$

This implies that $\theta_s = \theta_{\mathcal{A}}$.

Similar analysis shows that, if the contact point is in $\mathcal{B}$, the local contact angle will be $\theta_s = \theta_{\mathcal{B}}$.

Now we consider the case when the contact point is in $\mathcal{R}$. In this case, the energy I_0 is not smooth in τ and we could only compute the left and right derivative of I_0. Suppose that the material on the left of $z(\tau)$ is $\mathcal{A}$, and the material on the right is $\mathcal{B}$.

Then we could compute the left derivative as

$$\begin{aligned}\frac{\partial I_0}{\partial \tau}\Big|_- &= \sigma\frac{\partial L}{\partial \tau} + \frac{\partial}{\partial \tau}\Big|_-\left(\int_{\partial\Omega_1\cap\partial\Omega}\gamma(\mathbf{x},1)ds\right) + \frac{\partial}{\partial \tau}\Big|_-\left(\int_{\partial\Omega\setminus\partial\Omega_1}\gamma(\mathbf{x},-1)ds\right)\\ &= -\sigma\cos\theta + \gamma_{\mathcal{A}}(1) - \gamma_{\mathcal{A}}(-1)\\ &= \cos\theta_s - \cos\theta_{\mathcal{A}},\end{aligned} \tag{4.14}$$

and the right derivative as

$$\begin{aligned}\frac{\partial I_0}{\partial \tau}\Big|_+ &= \sigma\frac{\partial L}{\partial \tau} + \frac{\partial}{\partial \tau}\Big|_+\left(\int_{\partial\Omega_1\cap\partial\Omega}\gamma(\mathbf{x},1)ds\right) + \frac{\partial}{\partial \tau}\Big|_+\left(\int_{\partial\Omega\setminus\partial\Omega_1}\gamma(\mathbf{x},-1)ds\right)\\ &= -\sigma\cos\theta + \gamma_{\mathcal{B}}(1) - \gamma_{\mathcal{B}}(-1)\\ &= \cos\theta_s - \cos\theta_{\mathcal{B}}.\end{aligned} \tag{4.15}$$

Since I_0 is a minimizer, we must have

$$\frac{\partial I_0}{\partial \varsigma}|_- \le 0, \quad \frac{\partial I_0}{\partial \varsigma}|_+ \ge 0. \tag{4.16}$$

This implies the following condition for the contact angles,

$$\theta_{\mathcal{A}} \le \theta_s \le \theta_{\mathcal{B}}. \tag{4.17}$$

The situation for $z(\varsigma)$ can be proved in a similar way. This completes our proof. □

REMARK 4.2. *In the proof of the theorem, we did not consider the situation when the material on the left of $z(\tau)$ is $\mathcal{B}$, and the material on the right is $\mathcal{A}$. In fact, for a ϕ corresponding to such a configuration, we always have*

$$\frac{\partial I_0(\phi)}{\partial \tau}|_- = \cos\theta_s - \cos\theta_{\mathcal{B}} > \cos\theta_s - \cos\theta_{\mathcal{A}} = \frac{\partial I_0(\phi)}{\partial \tau}|_+.$$

This means that the function ϕ can not be a local minimizer in this case. As we will see in the examples in next section, the contact line jumps at such point.

5. Some examples for wetting hysteresis. The results in the previous sections provide a clear geometric picture of the equilibrium configuration in two dimensions. This enables us to explicitly calculate and minimize the total surface energy for some two-phase fluid systems with simple geometry. By considering the quasi-static motion of the interface on the patterned surfaces, described by the change of volume (or volume fraction), we can follow the change of the energy landscape, the change of contact angles and contact angle hysteresis. In this section, we study two explicit examples: the Poiseuille type flow on a patterned surface and a drop spreading on a patterned surface.

5.1. Quasi-static flow in a chemically patterned channel. We first consider a two phase quasi-static flow in a channel as shown in figure 5.1. The height of the channel is $2h$. The length of the channel is $2L$ with the lower side denoted by AC and the middle point denoted by B. In the following examples, we always choose $h = 4, L = 10$. The channel is patterned with two materials with equal length AB and BC with contact angles $\theta_{\mathcal{A}}$ and $\theta_{\mathcal{B}}$ respectively. The fluid interface energy density is given by γ. Denote the domain occupied by fluid 1 as Ω_1, and the domain occupied

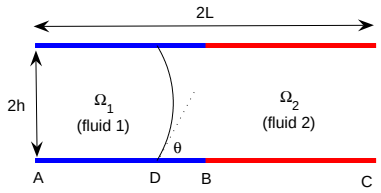

FIG. 5.1. *The channel consists of two materials.*

by fluid 2 as Ω_2. The results from the previous sections show that the interface is part of a circle with a contact point D on the lower side and a contact angle of fluid 2 on the solid surface θ. The length of the interval AD is denoted by x. The difference of the areas are measured by a parameter α defined as following:

$$|\Omega_1| - |\Omega_2| = \alpha \cdot (2L) \cdot (2h) \tag{5.1}$$

so that $-1 < \alpha < 1$. From (5.1), it is easy to show that x is related to θ as,

$$x = L - \frac{1}{2}\frac{h}{\cos^2\theta}\Big((\frac{\pi}{2} - \theta) - \cos\theta\sin\theta\Big) + \alpha L.$$

or equivalently

$$\hat{x} = \frac{x - L}{h} = -\frac{1}{2\cos^2\theta}\Big(\frac{\pi}{2} - \theta - \cos\theta\sin\theta\Big) + \alpha\frac{L}{h}. \tag{5.2}$$

Notice that for any fixed α, $\hat{x}$ is monotone-increasing function of θ.

We denote Σ_0, Σ_1 and Σ_2 the fluid-fluid interface, solid-fluid1 interface and solid-fluid2 interface, respectively. Notice that $\cos\theta_{\mathcal{A}} = \frac{\gamma_{1,\mathcal{A}} - \gamma_{2,\mathcal{A}}}{\gamma}$ and $\cos\theta_{\mathcal{B}} = \frac{\gamma_{1,\mathcal{B}} - \gamma_{2,\mathcal{B}}}{\gamma}$. Then, the normalized total surface energy of the system can then be calculated in terms of θ and α:

$$\hat{E}(\theta,\alpha) = \frac{E}{\gamma h} = \frac{\gamma|\Sigma_0| + \gamma_1|\Sigma_1| + \gamma_2|\Sigma_2|}{\gamma h} = \frac{(\pi - 2\theta)}{\cos\theta} + 2\hat{x}\beta + e_0 \tag{5.3}$$

where e_0 is a constant independent of θ and α, $\hat{x}$ is given by (5.2) and

$$\beta = \begin{cases} \cos\theta_{\mathcal{A}} & \text{if } \hat{x} < 0; \\ \cos\theta_{\mathcal{B}} & \text{if } \hat{x} > 0; \end{cases}$$

To understand the stick-slip motion of the interface and the contact angle hysteresis, we consider quasi-static motion of the interface as α changes. The increasing or decreasing of parameter α then correspond to the right or left motion of the interface. For each fixed α, the stable configurations can be obtained from locally minimizing the normalized total surface energy (5.3) with respect to θ. The corresponding contact point $\hat{x}$ and contact angle θ_s are also obtained. We study separately the stick ($\theta_{\mathcal{A}} > \theta_{\mathcal{B}}$) and slip ($\theta_{\mathcal{A}} < \theta_{\mathcal{B}}$) cases.

Contact line slip. We first consider the case when $\theta_{\mathcal{A}} < \theta_{\mathcal{B}}$. In the upper row of the Figure 5.2, we plot $\hat{E}(\theta, \alpha)$ as a function of θ for different values of α. It is easy to show that there are two critical α values

$$\alpha_- = \frac{h}{2L}(\frac{\pi/2 - \theta_{\mathcal{B}}}{\cos^2(\theta_{\mathcal{B}})} - \tan(\theta_{\mathcal{B}})), \qquad \alpha_+ = \frac{h}{2L}(\frac{\pi/2 - \theta_{\mathcal{A}}}{\cos^2(\theta_{\mathcal{A}})} - \tan(\theta_{\mathcal{A}}))$$

such that the normalized energy $\hat{E}(\theta, \alpha)$ experiences a transition from a single well function (in θ) to a double well function (or vise versa) at α_- and α_+. For $\alpha < \alpha_-$, $\hat{E}$ has a unique minimum at $\theta_{\mathcal{A}}$. For $\alpha_- < \alpha < \alpha_+$, $\hat{E}$ has two local minimums at $\theta_{\mathcal{A}}$ and $\theta_{\mathcal{B}}$. For $\alpha > \alpha_+$, $\hat{E}$ has a unique minimum at $\theta_{\mathcal{B}}$. The existence of multiple local minimum for $\hat{E}$ for $\alpha_- < \alpha < \alpha_+$ (i.e when the interface is close to the transition point of the pattern) is the origin for the contact angle hysteresis. In the lower row of the Figure 5.2, we plot the stable contact angle θ_s and the contact point $\hat{x}$ as the functions of α. As α increases (or interface moves from left to right)and passes α_-, the system chooses to stay in the same local minimum at the contact angle $\theta_{\mathcal{A}}$ since it costs energy to switch to the other minimum. When α passes α_+, $\theta_{\mathcal{A}}$ is no longer a local minimum and the contact angle has to switch instantly to $\theta_{\mathcal{B}}$ (which is now the only local minimum) as the contact point jumps a distance Δl where

$$\Delta l = \frac{h}{2}\left|(\frac{\pi/2 - \theta_{\mathcal{A}}}{\cos^2\theta_{\mathcal{A}}} - \frac{\pi/2 - \theta_{\mathcal{B}}}{\cos^2\theta_{\mathcal{B}}}) + (\tan\theta_{\mathcal{B}} - \tan\theta_{\mathcal{A}})\right|. \tag{5.4}$$

On the other hand, when the interface moves from right to left, the stable contact angle chooses to stay at $\theta_{\mathcal{B}}$ before it has to switch to $\theta_{\mathcal{A}}$ at $\alpha = \alpha_-$. We therefore observe hysteresis in both

Contact line pinning. The case when $\theta_{\mathcal{A}} > \theta_{\mathcal{B}}$ corresponds to the pinning (stick) of the interface. In Figure 5.3, we plot the energy $\hat{E}(\theta, \alpha)$ for different values of α in the upper row and stable contact angle θ_s and contact point $\hat{x}$ in the lower row. It is easy to see that $\hat{E}(\theta, \alpha)$ always has a unique minimum at θ_s for all α and

$$\theta_s = \begin{cases} \theta_{\mathcal{A}} & \text{if } \alpha \le \alpha_- \\ \theta_s \text{ determined by (5.2) with } \hat{x} = 0, & \text{if } \alpha_- < \alpha < \alpha_+ \\ \theta_{\mathcal{B}}, & \text{if } \alpha \ge \alpha_+ \end{cases}$$

Here α_- and α_+ are now given by

$$\alpha_- = \frac{h}{2L}(\frac{\pi/2 - \theta_{\mathcal{A}}}{\cos^2(\theta_{\mathcal{A}})} - \tan(\theta_{\mathcal{A}})), \qquad \alpha_+ = \frac{h}{2L}(\frac{\pi/2 - \theta_{\mathcal{B}}}{\cos^2(\theta_{\mathcal{B}})} - \tan(\theta_{\mathcal{B}}))$$

As α increases (or as the interface moves from left to right) and reaches α_-, the interface is pinned at point B ($\hat{x} = 0$) as α continues to increase from α_- to α_+ and the contact angle switches gradually from $\theta_{\mathcal{A}}$ to $\theta_{\mathcal{B}}$. As α decreases (or the interface goes back from right to left), it follows exactly the same path. The contact point is pinned at the same position and the contact angle switches gradually from $\theta_{\mathcal{B}}$ to $\theta_{\mathcal{A}}$. No hysteresis is observed in this case.

We next consider a channel periodically patterned with materials with different contact angles $\theta_{\mathcal{A}}$ and $\theta_{\mathcal{B}}$ on the solid boundary (Figure 5.4). We assume there are k periodic patterns in the interval $[\frac{L}{2}, \frac{L}{2}]$. In each period, the two materials occupies

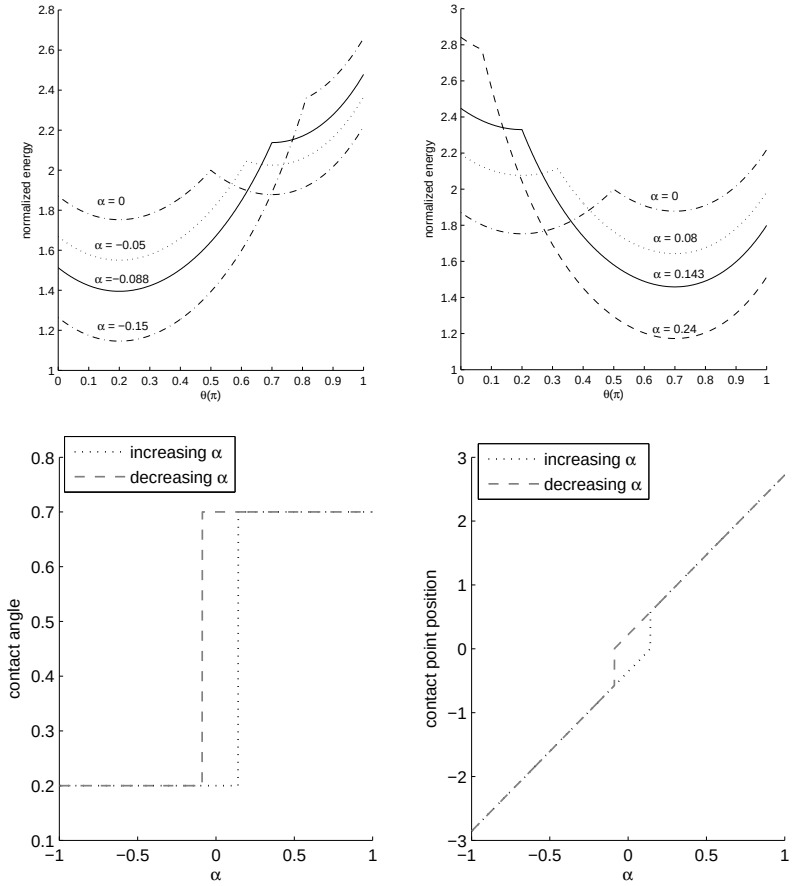

FIG. 5.2. *Contact angle hysteresis and contact line slipping. Upper row: The normalized energy (5.3) as functions of θ for different α. The solid lines are $\hat{E}(\theta)$ at α_- and α_+. Lower row: contact angle (left) and contact point(right) as functions of α. Here $\theta_{\mathcal{A}} = \frac{\pi}{5}, \theta_{\mathcal{B}} = \frac{7\pi}{10}$, $\alpha_- = -0.088$ and $\alpha_+ = 0.143$*

the same area $\Delta x = \frac{L}{2k}$. The normalized energy can be computed as the following:

$$\hat{E} = e_0 + \begin{cases} \frac{\pi-2\theta}{\cos\theta} + 2\hat{x}\cos\theta_{\mathcal{A}}, & \hat{x} \le -\frac{L}{2h}; \\ \frac{\pi-2\theta}{\cos\theta} - \frac{(L-2\Delta x)\cos\theta_{\mathcal{A}}}{h} + \frac{2I_x\Delta x(\cos\theta_{\mathcal{A}}+\cos\theta_{\mathcal{B}})}{h} & \\ \qquad +2(\hat{x} - \frac{(2I_x+1)\Delta x}{h} + \frac{L}{2h})\hat{\beta}, & -\frac{L}{2h} \le \hat{x} \le \frac{L}{2h}; \\ \frac{\pi-2\theta}{\cos\theta} + 2\hat{x}\cos\theta_{\mathcal{B}}, & \hat{x} \ge \frac{L}{2h}. \end{cases} \tag{5.5}$$

where $I_x = \left[\frac{2\hat{x}h+L}{4\Delta x}\right]$ is the integer part of the number $\frac{2\hat{x}h+L}{4\Delta x} = \frac{x-L/2}{2\Delta x}$, representing the number of complete periods occupied by fluid 1, and

$$\hat{\beta} = \begin{cases} \cos\theta_{\mathcal{A}} & \text{if } \frac{2\hat{x}h+L}{4\Delta x} - I_x \le \frac{1}{2}; \\ \cos\theta_{\mathcal{B}}, & \text{otherwise.} \end{cases}$$

In the examples below, we take $\theta_{\mathcal{A}} = \frac{\pi}{5}$ and $\theta_{\mathcal{B}} = \frac{7\pi}{10}$.

We now study the behavior of the quasistatic motion of the interface as the period k increases (or as the size of the pattern Δx decreases). Three different cases

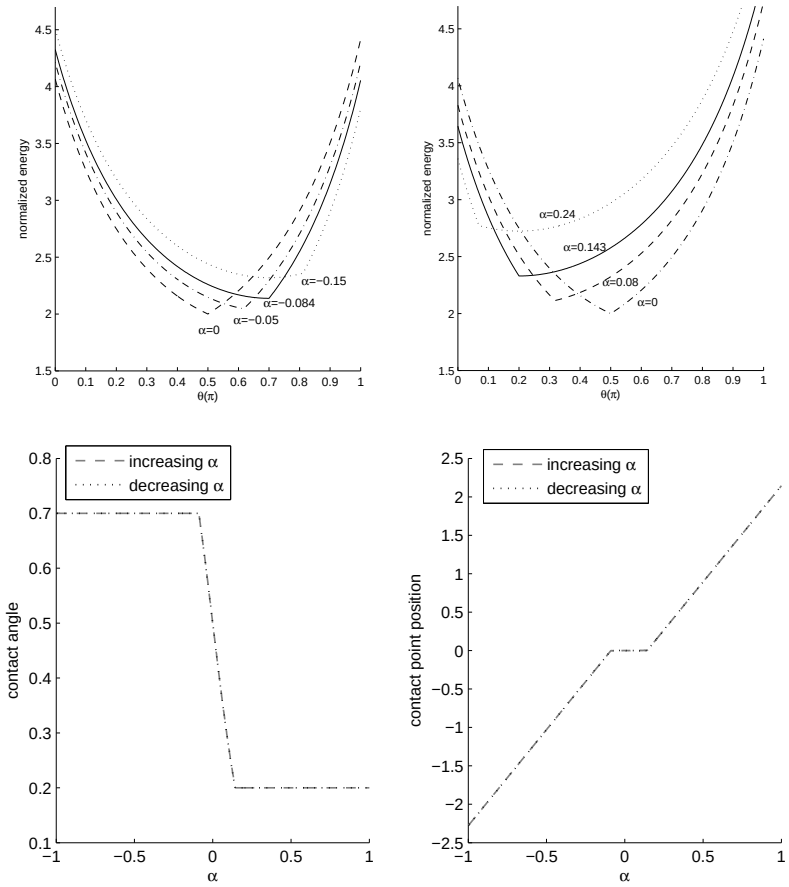

FIG. 5.3. *Contact line pinning. Upper row: The normalized energy as functions of θ (5.3) for different α. Lower row: contact angle (left) and contact point(right) as functions of α. Here $\theta_{\mathcal{A}} = \frac{7\pi}{10}, \theta_{\mathcal{B}} = \frac{\pi}{5}$, $\alpha_- = -0.088$ and $\alpha_+ = 0.143$*

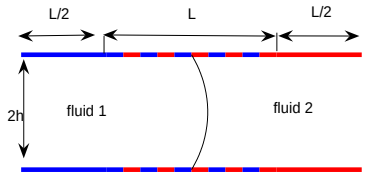

FIG. 5.4. *The chemically patterned channels*

are shown in Figure 5.5 ($k = 2$), Figure 5.6 ($k = 5$) and Figure 5.7 ($k = 15$) where the

contact angle θ_s and the contact point $\hat{x}$ are plotted as a function of α. For $k = 2$, the behavior of the interface is a simple repeat of the stick-slip behavior described in Fig. 5.3. For $k = 5, 15$, we see that the amplitude of the stick-slip becomes weaker as the size of the pattern Δx decreases. When $\Delta x < \Delta l$, the contact angle cannot switch completely between $\theta_{\mathcal{A}}$ and $\theta_{\mathcal{B}}$ because there is no room for such a switching. In fact, as Δx becomes smaller and smaller, the contact angle oscillates around $\theta_{\mathcal{B}}$ (or $\theta_{\mathcal{A}}$) as the interface moves to the left (or to the right), displaying apparent advancing (or receeding) contact angle (Figure 5.6 5.7) .

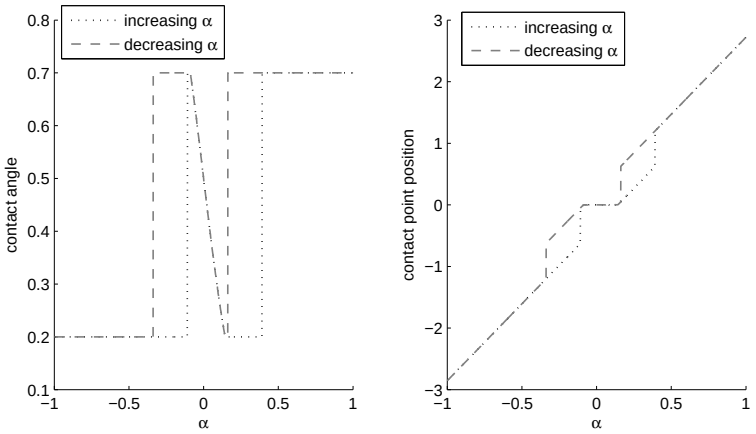

FIG. 5.5. *The contact angle and contact point as functions of α with $k = 2$. A simple repeat of the stick-slip motion and contact angle switching and contact angle hysteresis. $\theta_{\mathcal{A}} = \frac{\pi}{5}$, $\theta_{\mathcal{B}} = \frac{7\pi}{10}$.*

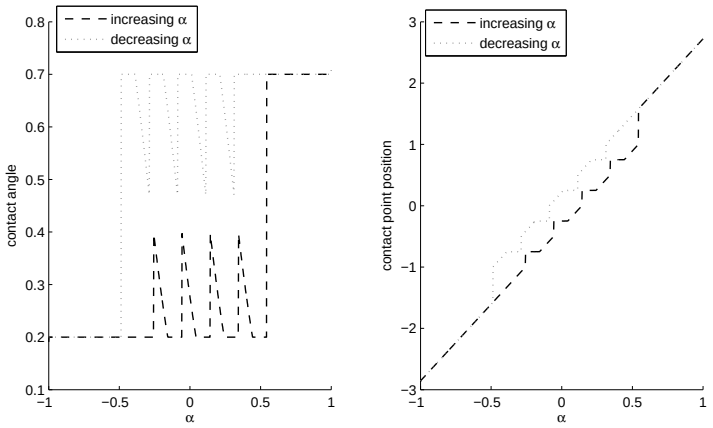

FIG. 5.6. *The contact angle and contact point as functions of α with $k = 5$. Here the pattern size $\Delta x < \Delta l$ so that contact angle will not switch. $\theta_{\mathcal{A}} = \frac{\pi}{5}$, $\theta_{\mathcal{B}} = \frac{7\pi}{10}$.*

5.2. A drop spreading on a patterned surface. We now study the hysteresis behavior of a drop spreading on a patterned surface. We assume that the surface is periodically patterned in the interval $(-R, R)$ as shown in Figure 5.8. We assume that the interval $(-R, R)$ is divided into $k + \frac{1}{2}$ periods with equal partition of two materials. The half period in the center is occupied by the material $\mathcal{B}$. Let $\Delta x = \frac{2R}{4k+1}$

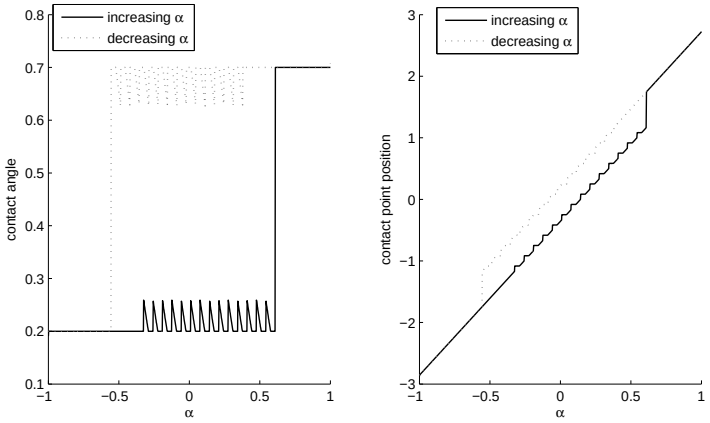

FIG. 5.7. *The contact angle and contact point as functions of α with $k = 15$. Here the pattern size is small enough so that one observes clear advancing and receding contact angles.* $\theta_{\mathcal{A}} = \frac{\pi}{5}$,$\theta_{\mathcal{B}} = \frac{7\pi}{10}$.

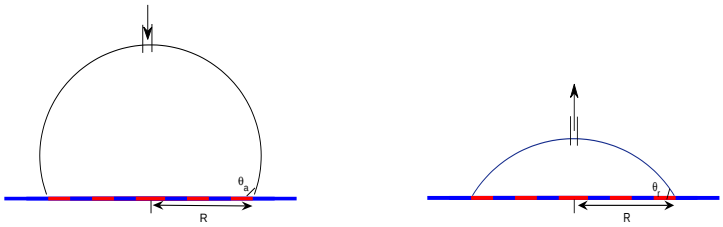

(a) advancing angle (b) advancing angle

FIG. 5.8. *Drop spreading and receding on patterned surface*

denote the length of a half period. Let r be the radius of the drop on the solid surface and θ be the contact angle. Then for any fixed drop volume V, r will be a function of the contact angle θ and the total surface energy E will also be a function of $r(\theta)$ and θ. We then compute the normalized radius $\hat{r}$,

$$\hat{r} = \frac{r}{R} = \frac{\sqrt{V}\sin\theta}{R\sqrt{\theta - \sin\theta\cos\theta}}, \tag{5.6}$$

The total normalized energy can be computed as

$$\hat{E}(\theta, V) = \frac{E}{2\gamma R} = e_1 + \frac{\hat{r}\theta}{\sin\theta} + \begin{cases} -\hat{r}\cos\theta_{\mathcal{B}}, & \hat{r} < \frac{\Delta x}{2R}; \\ -(\hat{r} - \frac{(4I_r+3)\Delta x}{2R})\beta - \frac{(\cos\theta_{\mathcal{A}}+\cos\theta_{\mathcal{B}})(1+2I_r)\Delta x}{2R} & \\ \qquad - \frac{\Delta x\cos\theta_{\mathcal{A}}}{2R}, & \frac{\Delta x}{2R} \le \hat{r} \le 1; \\ -\hat{r}\cos\theta_{\mathcal{A}} + \frac{2\hat{r}+\Delta x/R}{4}(\cos\theta_{\mathcal{A}} - \cos\theta_{\mathcal{B}}), & \hat{r} \ge 1. \end{cases} \tag{5.7}$$

where e_1 is a constant independent of V and θ, $I_r = \left[\frac{2r-\Delta x}{4\Delta x}\right]$ is the integer part of the number $\frac{r-\Delta x/2}{2\Delta x}$, representing the number of complete periods contained in the distance r, and

$$\beta = \begin{cases} \cos\theta_{\mathcal{A}}, & \text{if } \frac{2r-\Delta x}{4\Delta x} - I_r \le \frac{1}{2}; \\ \cos\theta_{\mathcal{B}}, & \text{otherwise.} \end{cases}$$

In Figure 5.9 ($k = 1$) and Figure 5.10 ($k = 15$), we plot the contact angle θ_s and the contact point $\hat{x}$ as functions of the volume V (in log scale). In both cases, we take $\theta_{\mathcal{A}} = \frac{\pi}{5}$ and $\theta_{\mathcal{B}} = \frac{7\pi}{10}$. The phenomena here are similar to that described in the previous section for the channel flow. For $k = 1$, the contact point goes through stick-slip motion and the contact angle switches between $\theta_{\mathcal{A}}$ and $\theta_{\mathcal{B}}$ displaying hysteresis. When the scale of the pattern is small (for $k = 15$), we observe weaker stick-slip but stronger hysteresis displaying the advancing contact angle $\theta_{\mathcal{B}}$ when the volume of the drop is increasing, and the receding contact angle $\theta_{\mathcal{A}}$ when the volume of the drop is decreasing. However, in the drop spreading case, the amount of the contact point jump Δl (when experiencing a complete switching between $\theta_{\mathcal{A}}$ and $\theta_{\mathcal{B}}$) is volume dependent and is given by

$$\Delta l = \sqrt{V}\left|\frac{\sin\theta_{\mathcal{B}}}{\sqrt{\theta_{\mathcal{B}} - \sin\theta_{\mathcal{B}}\cos\theta_{\mathcal{B}}}} - \frac{\sin\theta_{\mathcal{A}}}{\sqrt{\theta_{\mathcal{A}} - \sin\theta_{\mathcal{A}}\cos\theta_{\mathcal{A}}}}\right| \tag{5.8}$$

Therefore the oscillations near the advancing and receding angles not only decrease with size of the pattern Δx but also decrease with volume of the drop V.

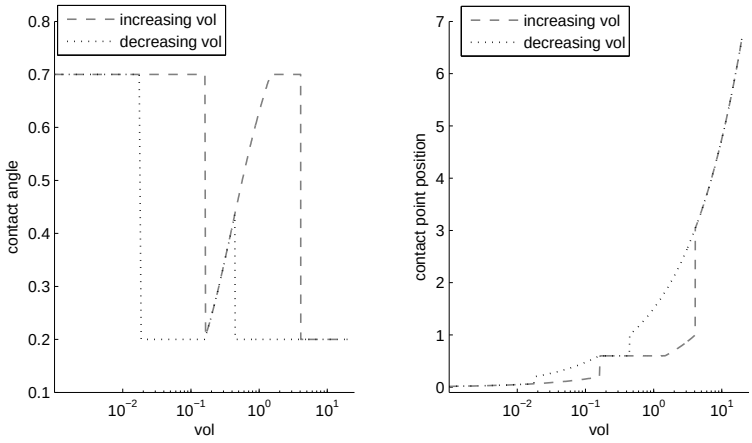

FIG. 5.9. *The contact angle hysteresis and stick-slip motion of a drop with* $k = 1$. $\theta_{\mathcal{A}} = \frac{\pi}{5}$, $\theta_{\mathcal{B}} = \frac{7\pi}{10}$.

Acknowledgments. This publication was based on work supported in part by Award No SA-C0040/UK-C0016, made by King Abdullah University of Science and Technology (KAUST), Hong Kong RGC-GRF grants 603107 and 604209 and the national basic research program under project of china under project 2009CB623200 , The first author would also like to thank the support by NSFC project 11001260 and the State Key Laboratory of Scientific and Engineering Computing of China

Appendix. *Proof of Proposition 4.1.* We only need to prove the following two lemmas for the lower-bound and upper-bound inequalities of Γ-convergence [3, 8].

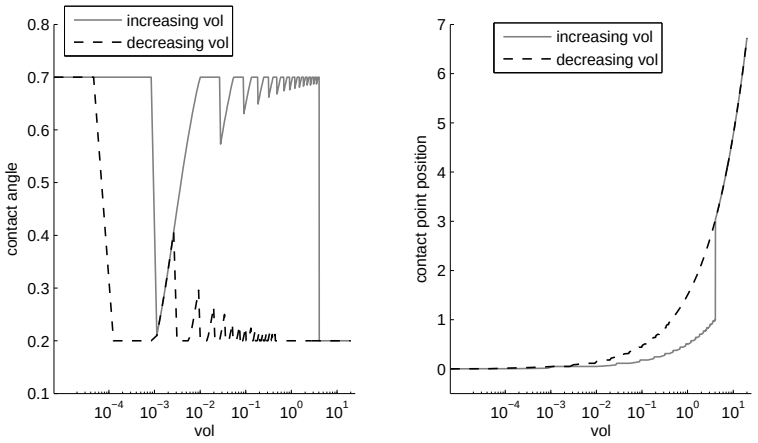

FIG. 5.10. *The contact angle hysteresis displaying advancing and receding contact angles. Here* $k = 15$. $\theta_{\mathcal{A}} = \frac{\pi}{5}$, $\theta_{\mathcal{B}} = \frac{7\pi}{10}$

Lemma A.1.(The lower-bound inequality) *For any* $\phi_\epsilon \in BV(\Omega)$, *if* $\phi_\epsilon \to \phi_0$ *in* $L^1(\Omega)$ *and* $\liminf_{\epsilon\to 0} I_\epsilon(\phi_\epsilon) < \infty$, *then we have:* $\phi_0 \in BV(\Omega)$, $\phi_0 = \pm 1, a.e.$, $\int_\Omega \phi = C_0$ *and*

$$\tilde{I}_0(\phi_0) \le \liminf_{\epsilon\to 0} I_\epsilon(\phi_\epsilon). \tag{A.1}$$

Proof. Since $\phi_\epsilon \to \phi_0$ in L^1, we can choose a subsequence (still denoted by ϕ_ϵ) such that $\phi_\epsilon \to \phi$ almost everywhere $x \in \Omega$. So $f(\phi_\epsilon) \to f(\phi), a.e. x \in \Omega$. By Fatou's lemma, we have

$$\int_\Omega f(\phi_0)dx \le \liminf_{\epsilon\to 0} \int_\Omega f(\phi_\epsilon) \le \liminf_{\epsilon\to 0} \epsilon I(\phi_\epsilon) = 0.$$

Notice that $f(\phi_0) \ge 0$, we have $f(\phi_0(x)) = 0, a.e.\ x \in \Omega$. This implies that $\phi_0 = \pm 1,\ x \in \Omega$.

Notice that $I_\epsilon(\phi_\epsilon) < \infty$, from the definition of the I_ϵ, we know that $\int_\Omega \phi_\epsilon = C_0$, notice again $\phi_\epsilon \to \phi_0$ in $L^1(\Omega)$, we have $\int_\Omega \phi_0 = C_0$.

To prove the lower-bound inequality (A.1), we define the function

$$F(t) = \int_{-1}^{t} (2f(r))^{\frac{1}{2}} dr.$$

We then have

$$\begin{aligned}\int_\Omega |DF(\phi_\epsilon)|dx &\le \int_\Omega |F'(\phi_\epsilon)||\nabla\phi_\epsilon|dx \\ &= \int_\Omega (2f(\phi_\epsilon))^{\frac{1}{2}}|\nabla\phi_\epsilon|dx \\ &\le \int_\Omega \epsilon f(\phi_\epsilon) + \frac{|\nabla\phi_\epsilon|^2}{2\epsilon}dx.\end{aligned}$$

Using the inequality $\tilde{\gamma}(x,\phi) \le \gamma(x,\phi)$, we have

$$\int_\Omega |DF(\phi_\epsilon)|dx + \int_{\partial\Omega} \tilde{\gamma}(x,\phi_\epsilon)ds \le I_\epsilon(\phi_\epsilon) < \infty.$$

In addition, similar to Proposition 1.4 in [17], we can show that $F(\phi_0) \in BV(\Omega)$ and

$$\int_\Omega |DF(\phi_0)|dx + \int_{\partial\Omega} \tilde{\gamma}(x,\phi_0)ds \le \liminf_{\epsilon\to 0} \int_\Omega |DF(\phi_\epsilon)|dx + \int_{\partial\Omega} \tilde{\gamma}(x,\phi_\epsilon)ds \le \liminf_{\epsilon\to 0} I_\epsilon(\phi_\epsilon).$$

Notice also that

$$\int_\Omega |DF(\phi_0)|dx = \int_{-\infty}^{+\infty} P_\Omega(\{x\in\Omega : F(\phi_0(x)) > t\})dt = \int_{F(-1)}^{F(1)} P_{\Omega_1} dt = \tilde{\sigma}|\partial\Omega_1 \cap \Omega|,$$

with $P_\Omega(\tilde{\Omega}) = |\partial\tilde{\Omega} \cap \Omega|$ and $\Omega_1 = \{x \in \Omega : \phi_0(x) = 1\}$. We have $\phi_0 \in BV(\Omega)$ and $\tilde{I}_0(\Omega_0) \le \liminf_{\epsilon\to 0} I_\epsilon(\phi_\epsilon)$. □

Remark A.1 The original version of Proposition 1.4 in [17] is for the homogeneous boundary condition. This is

$$\int_\Omega |DF(\phi_0)|dx + \int_{\partial\Omega} \tilde{\gamma}(\phi_0)ds \le \liminf_{\epsilon\to 0} \int_\Omega |DF(\phi_\epsilon)|dx + \int_{\partial\Omega} \tilde{\gamma}(\phi)ds.$$

However, this result is also true for the inhomogeneous boundary condition $\tilde{\gamma}(x,\phi)$. The reason is that the proof is Proposition 1.4 in [17] is based on Proposition 1.2 in the same paper, which is originally for the general boundary condition $\tilde{\gamma}(x,\phi)$.

Lemma A.2.(The upper-bound inequality) *For any* $\phi_0 \in BV(\Omega)$,$\phi_0 = \pm 1, a.e. x \in \Omega$, $\int_\Omega \phi_0 dx = C_0$, *such that* $I_0(\phi_0) < \infty$, *we have*

$$\limsup_{\epsilon\to 0^+} \inf_{\phi\in U_r(\phi_0)} I_\epsilon(\phi) \le I_0(\phi_0),$$

with

$$U_r(\phi_0) = \{\phi \in H^1(\Omega) : \|\phi - \phi_0\|_{L^2(\Omega)} < r, \int_\Omega \phi dx = \int_\Omega \phi_0 dx\}.$$

Proof. For any $\phi_0 \in BV(\Omega)$,$\phi_0 = \pm 1, a.e. x \in \Omega$, $\int_\Omega \phi_0 dx = C_0$, we set $\Omega_1 = \{x \in \Omega : \phi(x) = 1\}$. As in [17], we could construct a sequence $\tilde{\phi}_\epsilon$, which is also shown in Figure A.1. Let $\Gamma = \partial\Omega_1 \cap \Omega$, $\Omega_2 = \Omega \setminus \Omega_1$. The domain Ω is divided into several parts:

$A_1 = \Omega_1 \cap \{x \in \Omega, d(x,\partial\Omega) > C_1\epsilon\}$;
$A_2 = (\Omega_2 \cap \{x \in \Omega, d(x,\partial\Omega) > C_1\epsilon\} \cap \{x \in \Omega, d(x,\Gamma) > C_1\epsilon\}) \setminus B_\epsilon$;
with $B_\epsilon = \{x \in \Omega_2 : |x - x_0| < \epsilon^{1/2}\}$ for some $x_0 \in \Omega_2, d(x_0,\partial\Omega) > \epsilon^{\frac{1}{2}}$;
and other boundary layers.

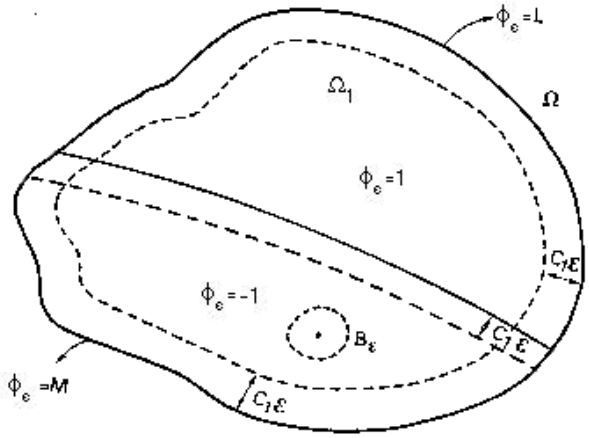

Figure A.1. The construction of ϕ_ϵ in [17].

The ϕ_ϵ is defined as

$$\phi_\epsilon(x) = \begin{cases} 1 & x \in A_1 \\ -1 & x \in A_2 \\ L & x \in \partial\Omega_1 \cap \partial\Omega \\ M & x \in \partial\Omega_2 \cap \partial\Omega \cap \{x \in \partial\Omega : d(x,\Gamma) > C_1\epsilon\} \end{cases}$$

ϕ_ϵ is set to some functions continuous to boundary in the boundary layers and in B_ϵ. For simplicity, we do not give the exact definition of these continuous functions. Readers who are interested are referred to the definitions in [17]. The constructed functions ϕ_ϵ are such that the following conditions(see in[17]):

$$\lim_{\epsilon\to 0}\int_\Omega |\phi_\epsilon - \phi_0|^2 dx = 1, \int_\Omega \phi_\epsilon dx = C_0.$$

and

$$\begin{aligned}\limsup_{\epsilon\to 0}\int_\Omega \epsilon|\nabla\phi_\epsilon|^2 + \frac{2}{\epsilon}f(\phi_\epsilon)dx \le 2|\partial\Omega_1\cap\Omega|\int_{-1}^{1}(\delta+2f(t))^{1/2}dt \\ +2|\partial\Omega_2\cap\partial\Omega|\Big|\int_{-1}^{M}(\delta+2f(t))^{1/2}dt\Big| \\ +2|\partial\Omega_1\cap\partial\Omega|\Big|\int_{1}^{L}(\delta+2f(t))^{1/2}dt\Big|.\end{aligned}$$

Here $\delta > 0$ is a number independent of L and M.

Thus, we have: for any $r > 0$,

$$\begin{aligned}
\limsup_{\epsilon\to_0}\inf_{\phi\in U_r(\phi_0)} I_\epsilon(\phi) &\le \limsup_{\epsilon\to_0} I_\epsilon(\phi_\epsilon)\\
&= \limsup_{\epsilon\to_0}\int_\Omega \frac{\epsilon}{2}|\nabla\phi_\epsilon|^2 + \frac{f(\phi_\epsilon)}{\epsilon}dx + \int_{\partial\Omega}\gamma(x,\phi_\epsilon)ds\\
&\le |\partial\Omega_1\cap\Omega|\int_{-1}^{1}(\delta+2f(t))^{1/2}dt\\
&\quad +|\partial\Omega_2\cap\partial\Omega|\Big|\int_{-1}^{M}(\delta+2f(t))^{1/2}dt\Big| + \int_{\partial\Omega_2\cap\partial\Omega}\gamma(x,M)ds\\
&\quad +|\partial\Omega_1\cap\partial\Omega|\Big|\int_{1}^{L}(\delta+2f(t))^{1/2}dt\Big| + \int_{\partial\Omega_1\cap\partial\Omega}\gamma(x,L)ds.
\end{aligned}$$

$$\begin{aligned}
&= |\partial\Omega_1\cap\Omega|\int_{-1}^{1}(\delta+2f(t))^{1/2}dt\\
&\quad + \int_{\partial\Omega_2\cap\partial\Omega}\Big|\int_{-1}^{M}(\delta+2f(t))^{1/2}dt\Big| + \gamma(x,M)ds\\
&\quad + \int_{\partial\Omega_1\cap\partial\Omega}\Big|\int_{1}^{L}(\delta+2f(t))^{1/2}dt\Big| + \gamma(x,L)ds.
\end{aligned}$$

Notice the left of the above inequality is independent of δ, M and L, we could take infimum with respect to these parameters on the right. Notice also the definition of $\tilde\gamma(x,\pm1)$, we get that

$$\begin{aligned}
\limsup_{\epsilon\to_0}\inf_{\phi\in U_r(\phi_0)} I_\epsilon(\phi) &\le |\partial\Omega_1\cap\Omega|\int_{-1}^{1}(2f(t))^{1/2}dt + \int_{\partial\Omega_2\cap\partial\Omega}\tilde\gamma(x,-1)ds\\
&\quad + \int_{\partial\Omega_1\cap\partial\Omega}\tilde\gamma(x,1)ds\\
&= I_0(\phi_0).
\end{aligned}$$

We have proved the upper-bound inequality. □

REFERENCES

[1] G. Alberti and A. DeSimone, *Wetting of rough surfaces: a homogenization approach*, Proc. R. Soc. A, 451 (2005) pp. 79-97.

[2] D. Bonn, J. Eggers, J. Indekeu, J. Meunier and E. Rolley, *Wetting and spreading*, Rev. Mod. Phy., 81 (2009) pp. 739-805.

[3] A. Braids,*Γ-convergence for beginners, Oxford Lecture Series in Mathematics and its Applications*, Vol. 22, Oxford University Press, 2002.

[4] G. Caginalp, *An analysis of a phase field model of a free boundary*, Arch. Rational Mech. Anal. 92 (1986) pp. 205-245.

[5] G. Caginalp and P. C. Fife,*Dynamics of layered interfaces arising from phase boundaries*, SIAM J. Appl. Math. 48 (1988) pp. 506-518.

[6] A. Cassie and S. Baxter,*Wettability of porous surfaces*, Trans. Faraday Soc., 40 (1944) pp. 546-551.

[7] X. Chen and M. Kowalczyk, *Existence of equillibria for the Cahn-Hilliard equation via local minimizers of the perimeter*, Comm. Partial Diff. Equ., 21 (1996) pp. 1207-1233.

[8] G. Dal Maso,*Introduction to Γ-convergence*, Birkhauser, 1993.

[9] A. DeSimone, N. Grunewald and F. Otto, *A new model for contact angle hysteresis*, Network and Heterogenneous Media, 2 (2007) pp. 211-225.
[10] E.B. Dussan, *On the spreading of liquids on solid surfaces: static and dynamic contact lines*, Ann. Rev. Fluid Mech. 11 (1997) pp. 371-400.
[11] P. G. de Gennes, *Wetting: statics and dynamics*, Rev. Mod. Phy., 57 (1985) pp. 827-863.
[12] E. Giusti,*Direct methods in the calculus of variations*, World Scientific, 2003.
[13] D. Jacqmin, *Contact-line dynamics of a diffuse fluid interface*, J. Fluid Mech. 402 (2000) pp. 57-88.
[14] H. Kusumaatmaja and J. M. Yeomans, *Modeling contact angle hysteresis on chemically pattered and superhydrophobic surfaces*, Langmuir, 23 (2007) pp. 6019-6032.
[15] R. V. Kohn and P. Sternberg, *Local minimizers and singular pertubations*, Proc. Roy. Soc. Edinburgh, 111A (1989) pp. 69-84.
[16] A. Marmur and E. Bittoun,*When Wenzel and Cassie Are Right: Reconciling Local and Global Considerations*, Langmuir, 25 (2009) pp. 1277-1281.
[17] L, Modica, *Gradient theory of phase transitions with boundary energy*, Ann. Inst. Henri Poincaré, 4 (1987) pp. 487-512.
[18] D. Quere, *Wetting and roughness*, Annu. Rev. Mater. Res., 38 (2008) pp. 71-99.
[19] J. Nevard and J. B. Keller,*Homogenization of rough boundaries and interfaces*, SIAM J. Appl. Math. 57 (1997) pp. 1660-1686.
[20] R. L. Pego, *Front migration in the nonlinear Cahn-Hilliard equation*, Proc. Roy. Soc. London A, 422 (1989) pp. 261-278.
[21] T. Qian, X.-P. Wang and P. Sheng, *Molecular scale contact line hydrodynamics of inmmiscible flows*, Phy. Rev. E., 68 (2003) 016306.
[22] A. Turco, F. Alouges and A. DeSimone, *Wetting on rough surfaces and contact angle hysteresis: numerical experiments based on a phase field model*, M2AN 43 (2009) pp. 1027-1044.
[23] S. Vedantam and M. V. Oanchagnula, *Constitutive modeling of contact angle hysteresis*, Journal Colliod and Interface Science, 321 (2008) pp. 393-400.
[24] X.-P. Wang, T. Qian and P. Sheng, *Moving contact line on chemically patterned surfaces*, Journal of Fluid Mechanics, 605 (2008) pp. 59-78
[25] X.-P. Wang and Y.-G. Wang, *The sharp interface limit of a phase field model for moving contact line problem*, Methods Appl. Anal. 14 (2007) pp. 285-292.
[26] R. N. Wenzel,*Resistance of solid surfaces to wetting by water*, Ind. Eng. Chem., 28 (1936), pp. 988-994.
[27] G. Whyman, E. Bormashenko and T. Stein, *The rigorous derivative of Young, Cassie-Baxter and Wenzel equations and the analysis of the contact angle hysteresis phenomenon*, Chem. Phy. Letters, 450 (2008) pp. 355-359.
[28] X. Xu and X.-P. Wang, Derivation of Wenzel's and Cassie's equations froma phase fieeld model for two phase flow on rough surface, SIAM J. Appl. Math, 70 (2010), pp. 2929-2941
[29] T. Young, *An essay on the cohesion of fluids*, Philos. Trans. R. Soc. London (1805), 95, pp. 65-87.
[30] P. Yue, C. Zhou, and J. Feng, *Sharp-interface limit of the Cahn-Hilliard model for moving contact lines*, J. Fluid Mech. (2010), 645, pp. 279-294.